7298–7307 Nucleic Acids Research, 2010, Vol. 38, No. 20 Published online 12 July 2010
doi:10.1093/nar/gkq621

Solution-state structure of a fully alternately 2′-F/2′-OMe modified 42-nt dimeric siRNA construct

Peter Podbevsek[1], Charles R. Allerson[2], Balkrishen Bhat[2] and Janez Plavec[1,3,4,*]

[1]Slovenian NMR Center, National Institute of Chemistry, Hajdrihova 19, SI-1001 Ljubljana, Slovenia, [2]Department of Medicinal Chemistry, Isis Phamaceuticals, Inc., 1896 Rutherford Road, Carlsbad CA 92008, USA, [3]Faculty of Chemistry and Chemical Technology, University of Ljubljana and [4]EN-FIST Center of Excellence, SI-1000 Ljubljana, Slovenia

Received May 5, 2010; Revised June 21, 2010; Accepted June 27, 2010

ABSTRACT

A high-resolution solution structure of a stable 42-nt RNA dimeric construct has been derived based on a high number of NMR observables including nuclear overhauser effects (NOEs), J-coupling constants and residual dipolar couplings (RDCs), which were all obtained with isotopically unlabeled molecules. Two 21-nt siRNA that efficiently hybridize consist of ribose units that were alternately substituted by 2′-fluoro or 2′-methoxy groups. Structure calculations utilized a set of H-F RDC values for all 21 2′-fluoro modified nucleotides under conditions of weak alignment achieved by Pf1 phages. A completely 2′-F/2′-OMe modified dimeric RNA construct adopts an antiparallel double-helical structure consisting of 19 Watson–Crick base pairs with additional 3′ UU overhangs and a 5′ phosphate group on the antisense strand. NMR data suggest that the stability of individual base pairs is not uniform throughout the construct. While most of the double helical segment exhibits well dispersed imino resonances, the last three base pairs either display uncharacteristic chemical shifts of imino protons or absence of imino resonances even at lower temperatures. Accessibility of imino protons to solvent exchange suggests a difference in stability of duplex ends, which might be of importance for incorporation of the guide siRNA strand into a RISC.

INTRODUCTION

During recent years, it has become evident that small regulatory RNAs play an important role in many biological processes including control of mechanisms directing gene expression and thus can be exploited for various therapeutic purposes. An accidental discovery, which suggested that RNA can be used for silencing virtually any gene, has opened up a new field of gene therapy (1–5). The mechanism, termed RNA interference (RNAi), is triggered by short RNA duplexes (6–8). Naturally occurring siRNAs are produced by enzymatic cleavage of a longer double stranded RNA molecule into shorter RNA duplexes. siRNAs are typically 21-nt long and contain 2-nt 3′ overhangs and 5′ phosphates. Once in cells, siRNA associates with argonaute and other proteins forming an RNA-induced silencing complex (RISC) (9). One strand of the siRNA duplex is degraded, while the other strand stays bound to the RISC and base pairs with a messenger RNA (mRNA) containing the complementary sequence. The proteins within RISC possess nuclease activity and cleave the target mRNA at a single site. Binding of RNA to a complementary region on its target mRNA leads to gene silencing by translational repression and/or mRNA degradation. This reduces the level of target mRNA in cells and effectively knocks down a specific gene.

Since siRNAs can be artificially introduced into cells by various methods, RNAi has become a powerful tool for the regulation of gene expression. Unfortunately, the initial promises of the use of synthetic siRNAs consisting of solely standard nucleotides proved problematic. One of the main difficulties is the short half-life of unmodified RNA in serum due to the activity of endo- and exonucleases. In order to overcome the problem of instability against nuclease degradation, a variety of chemically modified nucleotides have been utilized in synthetic siRNAs (10–12). Earlier studies showed that the 2′-OH group is not required for siRNAs to elicit an RNAi response (13). Therefore, the 2′ position on the sugar moiety has been extensively modified. It has been shown that 2′-O-methyl (2′-OMe) (14) and 2′-deoxy-2′-fluoro

*To whom correspondence should be addressed. Tel: +386 1 4760353; Fax: +386 1 4760300; Email: janez.plavec@ki.si
Present address:
Balkrishen Bhat, Regulus Therapeutics, 1896 Rutherford Road, Carlsbad CA 92008, USA.

(2′-F) (15) modifications (Figure 1) increase the nuclease stability of siRNAs, and at the same time retain its RNAi activity. Second generation antisense oligonucleotides incorporating these 2′-modifications exhibit high binding affinity to the target RNA, enhanced metabolic stability, and improved pharmacokinetic and toxicity profiles (16). Several reports have discussed different extents of substitution with modified nucleotides ranging from just a single nucleotide to the use of uniform modification along both strands (12).

Recently, Bhat and coworkers identified a highly potent siRNA duplex, which targets the B site of the human phosphatase and tensin homolog mRNA, which was previously shown to be a target for degradation using the siRNA approach (17). The fully modified duplex, which is comprised of alternating 2′-F and 2′-OMe nucleotides exhibits several desirable pharmacokinetic properties (18). The melting temperature of the modified duplex is 20°C higher in comparison to an unmodified RNA oligonucleotide. High thermal stability is, at least in part, responsible for the significantly higher plasma stability observed in the modified siRNA. Consequently, 2′-F/2′-OMe siRNA showed a more than a 500-fold increase in *in vitro* potency versus unmodified siRNA (18,19).

2′-modifications can influence the sugar conformation to adopt a predominantly North-type (N) sugar pucker, and can also improve properties such as affinity (20–24). 2′-modifications that provide a gauche effect and/or a charge effect can play a significant role in the level of nuclease resistance. Interplay of stereoelectronic effects, sequence, hydration or metal ion interactions can influence equilibrium between canonical A- and B-type duplex and other conformations.

The focus of the current study is on a 42-nt dimeric RNA construct which consists of 19 Watson–Crick base pairs, 3′ UU overhangs in both strands, which are found in naturally occurring siRNAs, and a 5′ phosphate on the antisense strand, which is required for the correct positioning within the RISC (Figure 2). We attempt to analyze conformational preorganization of the two 21-nt RNAs separately and after hybridization into the dimeric construct by solution state NMR without the use of ^{13}C and ^{15}N isotope labeling. Structural characterization of the dimeric construct provides molecular details which correlate with the high potency of the modified siRNA. Overall topology and details of the 3D structure of the fully 2′-F/2′-OMe modified siRNA duplex together with the dynamics of individual segments offer deeper insights into structural features as well as the role of 3′ overhangs. At the outset, we expected to observe differences in duplex stability that would be localized to the specific section of the construct. Contiguous base pairs in the 5′ seed region and near the cleavage site are important for nuclease activity (25,26). Disruption of the helical duplex geometry may be important for intermolecular interactions of a RNA complex with its complementary region on a target mRNA which is at the heart of gene silencing by translational repression or degradation.

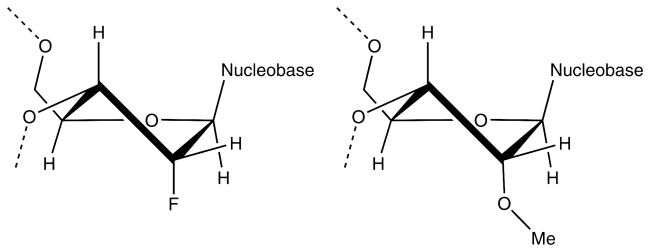

Figure 1. Schematic representation of 2′-deoxy-2′-fluoro (left) and 2′-OMe (right) substituted ribose units in the preferred N-type sugar conformation.

MATERIALS AND METHODS

Sample preparation and NMR data collection

The NMR sample was prepared by dissolving the oligonucleotides ISIS 401156 (5′-GGGUAAAUACAUUCUU CAUUU-3′) and ISIS 401157 (P-5′-AUGAAGAAUGUA UUUACCCUU-3′) in a 100% $^{2}H_2O$ or 5% $^{2}H_2O$, 95% H_2O aqueous solution containing 20 mM NaCl and 20 mM sodium phosphate buffer (pH = 6.8). Oligonucleotide concentration in the NMR sample was 2.0 mM per strand. The sample used to measure residual dipolar couplings (RDCs) was prepared by redissolving the NMR sample in a 100% $^{2}H_2O$ filamentous Pf1 phage solution (Asla Ltd). The total phage concentration was 17 mg/ml which resulted in a deuterium splitting of 17.1 Hz at 800 MHz. 1D ^{1}H and 2D NOESY, DQF-COSY and TOCSY NMR spectra were recorded on Varian VNMRS 800 MHz spectrometer equipped with a cold probe. DPFGSE water suppression scheme was used for suppression of the water signal. 2D HP-COSY spectra were recorded on a Varian VNMRS 600 MHz spectrometer with a penta probe. All experiments were performed on a natural abundance sample at temperatures ranging from 0 to 35°C. NMR spectra were processed and

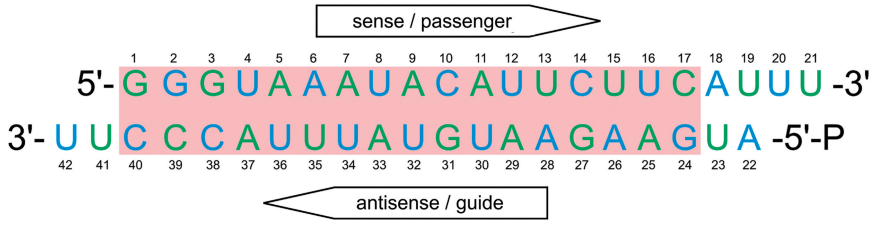

Figure 2. Base pairing pattern of the 2′-F/2′-OMe modified sense/passenger and antisense/guide RNA strands. 2′-F and 2′-OMe modified nucleotides are depicted in green and blue, respectively. The base paired segments of the strands that displayed observable imino resonances are shaded in red.

analyzed using VNMRJ (Varian Inc.) and Sparky software (UCSF).

T_m measurement

A solution for measuring the thermal stability of the fully-modified duplex was prepared by combining equal volumes of 8 μM solutions of each oligonucleotide in a buffer of 100 mM NaCl, 10 mM sodium phosphate (pH 7) and 0.1 M EDTA, yielding final concentration of 4 μM duplex. A Cary 100 Bio spectrophotometer with the Cary Win UV Thermal program was used to measure absorbance versus temperature. The solution was heated at 0.5°C/min from 15 to 95°C (repeated in triplicate), and T_m was determined from the A260 versus temperature curve.

Structure calculations

Structure calculations were performed using AMBER 9 software with the parmbsc0 force field (27). Force field parameters for the modified nucleotides were used from previous studies (28,29). Initial starting structure was created using the InsightII software. The structure was then subjected to 100 ps of NMR restrained simulated annealing (SA) calculations using a generalized Born implicit solvation model. For each SA calculation a random starting velocity was used. For the first 15 ms the molecules were held at a constant temperature of 300 K. The molecules were then heated to 1000 K in the next 10 ps, after which temperature was constant for 25 ps, scaled down to 100 K in the next 25 ps and reduced to 0 K in the last 25 ps. The force constants were 35 kcal mol^{-1} Å^{-2} for nuclear overhauser effect (NOE) distance, 300 kcal mol^{-1} rad^{-2} for torsion angle and 25 kcal mol^{-1} Å^{-2} for base planarity restraints. Direct dipolar HF coupling restraints were used to define the five unique elements of the alignment tensor. In the AMBER software, these elements are treated as additional variables and are optimized along with the structural parameters. The variables used are the Cartesian components of the alignment tensor in the axis system defined by the molecule itself. The alignment tensor was fitted to the starting structure, and the tensor obtained from this fitting was used as the initial guess for further refinement. The cutoff for non-bonded interactions was 20 Å. The SHAKE algorithm for hydrogen atoms was used with a tolerance of 0.0005 Å. All structures from SA were subjected to a maximum of 10 000 steps of steepest descent minimization. A family of 10 minimized structures with the lowest energy and the smallest NMR violations were selected for further analysis. Helical parameters were determined with 3DNA 2.0 software (30). We have also performed the structural calculations without the use of base planarity restraints. The convergence and overall RMSD of the final structures were comparable to the original set of structures. Analysis of local base-pair parameters showed that the average propeller twist changed from −6.7 (SD 0.6, maximum deviation per base pair 3.7°) to −10.1° (SD 1.2, maximum deviation per base pair 7.0°) with and without base planarity restraints, respectively. No other deviations in the two final families of structures could be observed.

Coordinate deposition

The coordinates for the family of the 10 lowest energy structures of the 2′-F/2′-OMe modified dimeric 42-nt construct have been deposited in the Protein Data Bank with the accession code 2KWG.

RESULTS

Single-strand preorganization

Solutions of individual 2′-F/2′-OMe modified 21-nt RNA oligonucleotides were prepared in 5% ^2H_2O, 95% H_2O and transferred into NMR tubes. 1D ^1H NMR spectrum of the sense strand exhibits three imino resonances at 15°C (Figure 3A and B). The resonance at δ12.4 p.p.m. reveals a slightly broader width at half-height in comparison to the remaining two resonances and undergoes significant broadening upon lowering the temperature to 0°C. The chemical shifts of the two sharp imino resonances suggest the formation of one AU and one GC base pair. Imino–imino cross-peak in NOESY spectrum (data not shown) indicates that the two base pairs are adjacent. The base pairing pattern can be associated with one of the topologies suggested by the MFOLD program (31) (Figure 3A). No NOESY cross-peaks at δ12.4 p.p.m. could be observed due to the broad nature of resonance signal.

Five imino resonances in the range from δ11.0 to 14.0 p.p.m. could be observed in the 1D ^1H NMR spectrum of the antisense strand at 15°C (Figure 3C and D). On the basis of chemical shifts, the two upfield imino resonances were assigned to a GU base pair, which was confirmed by the strong NOESY imino–imino cross-peak between them. The GU base pair is adjacent to an AU base pair with its imino proton resonating at δ14.0 p.p.m. The two remaining resonances at δ13.1 and 13.2 p.p.m. exhibit a NOESY cross-peak between each other, but no cross-peaks to other imino protons. The resonances at δ13.1 and 13.2 p.p.m. correspond to adjacent AU and GC base pairs, respectively. The base pairing pattern could be linked to one of the topologies suggested by the MFOLD program (31) (Figure 3C).

Dimeric construct exhibits well resolved NMR signals

Equimolar amounts of the two 2′-F/2′-OMe modified 21-nt RNA oligonucleotides in 5% ^2H_2O, 95% H_2O were transferred into an NMR tube. 1D ^1H 800 MHz NMR spectrum exhibited sharp and well resolved resonances (Figure 4). Seventeen imino resonances could be identified in the region from δ11.5 to 14.2 p.p.m. indicating Watson–Crick base pairing, which suggests the formation of a single double helical structure. A second sample of equimolar amounts of the 2′-F/2′-OMe oligonucleotides was prepared in phosphate buffer solution, and was used to measure the thermal hybridization stability (T_m) of the resulting duplex. A single hyperchromic transition was observed at 81.7°C,

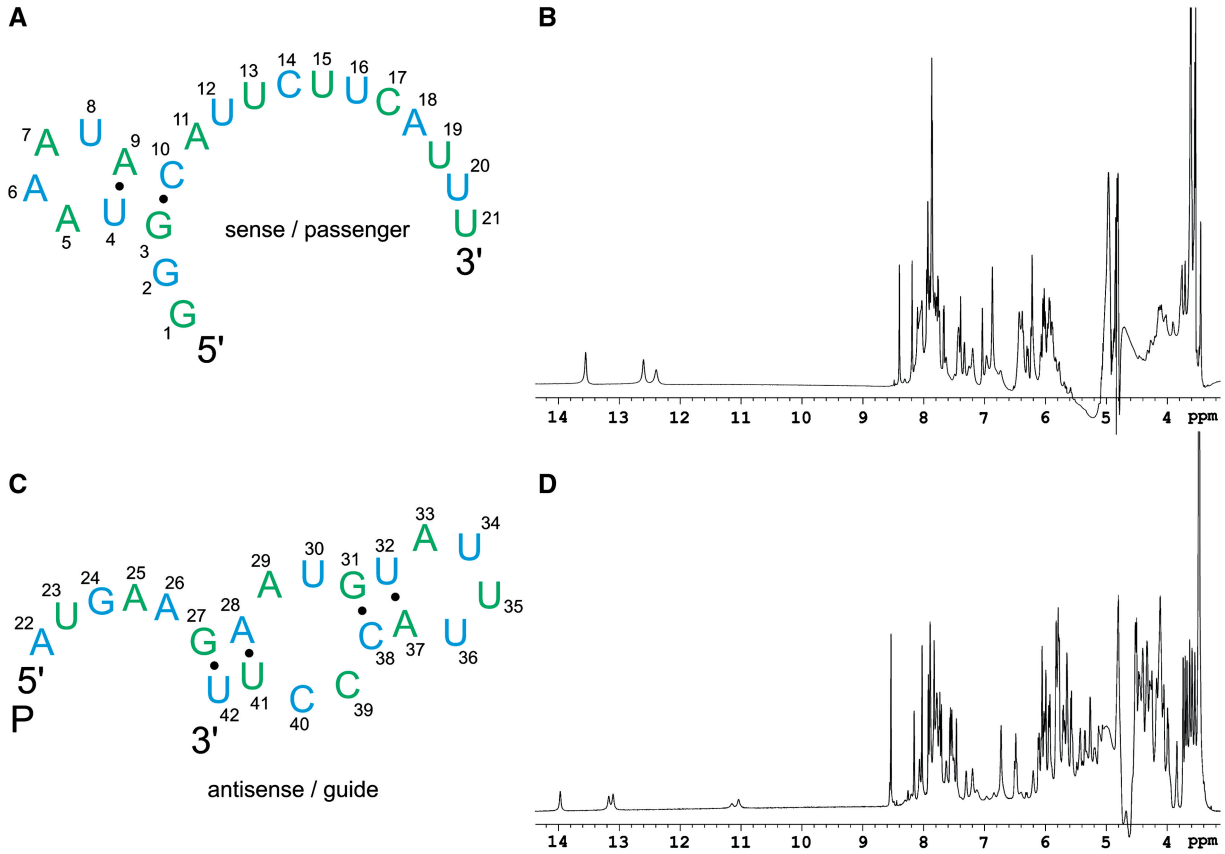

Figure 3. Base pairing pattern of the sense (**A**) and antisense (**C**) strands and the corresponding 1D ^{1}H NMR spectra of individual sense (**B**) and antisense (**D**) strands recorded at 15°C.

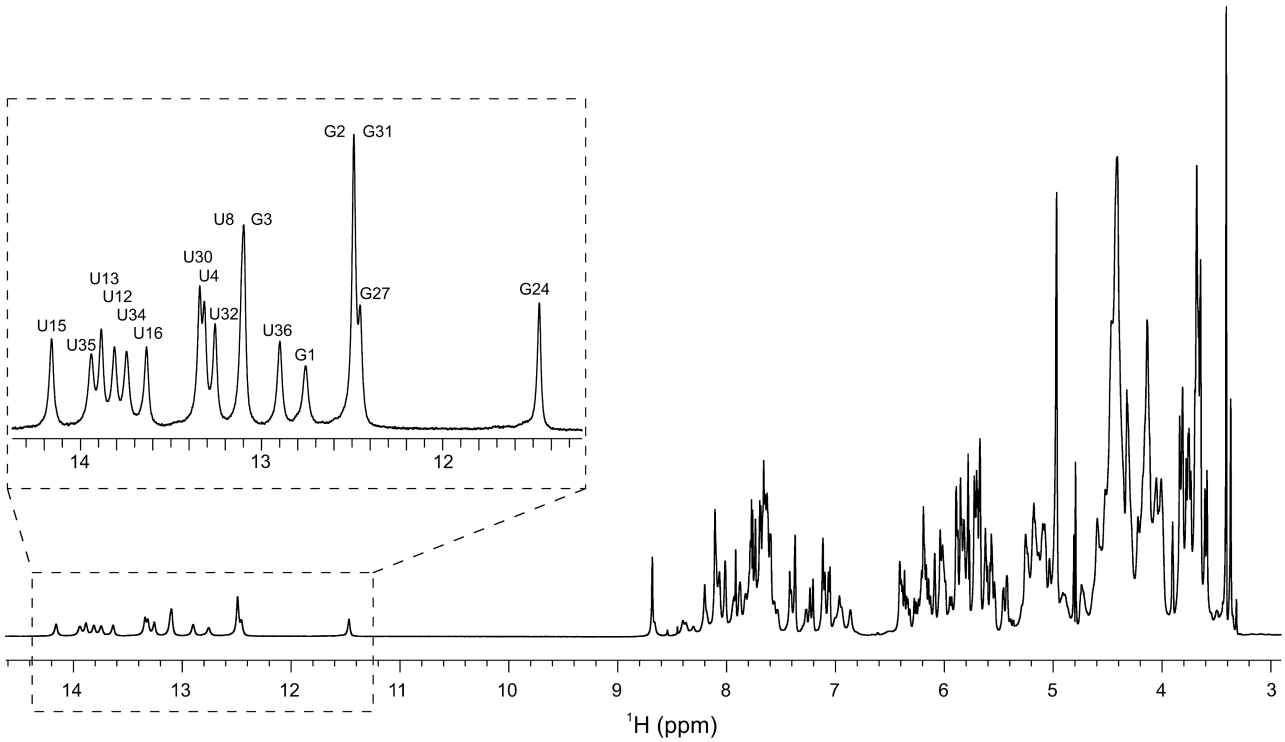

Figure 4. 1D ^{1}H NMR spectrum of the dimeric RNA construct recorded at 25°C. Imino region with the assignment of resonances is shown in the inset.

confirming the formation of a single base paired species. Detailed temperature-dependent NMR measurements were used to assess the local thermal stability of individual base pairs. The NMR melting profiles in temperature range from 25 to 80°C reveal that the melting of the duplex is not uniform and that base pairs located in the labile segment of the helix exhibit noticeably lower melting temperatures in comparison to the rest of the construct (Supplementary Figure S1). U15, U16 and G24 imino proton resonances which are resolved throughout the temperature range can be observed at temperatures of up to 55°C. On the other hand, G27 imino proton, which constitutes the next base pair is observed at temperatures of up to 70°C. Other imino resonances cannot be uniquely identified due to distinct temperature variation of their chemical shift and severe spectral overlap. They can be observed, however, at temperatures of up to 65°C. Interestingly, some imino peaks are observed even at 80°C.

Assignment of the imino resonances was possible through the imino–imino sequential walk in 2D NOESY spectra (Figure 5). The imino peaks indicated the formation of continuous Watson–Crick base pairs between G1-C40 and U16-A25 pairs. The additional C17·G24 base pair was inferred through the observation of G24 imino proton at the chemical shift of δ11.5 p.p.m. This chemical shift of a GC Watson–Crick base pair suggests specific stacking interactions or other structural features at the end of a perfectly hydrogen bonded double helix. The imino proton of a GC base pair flanked by a UA base pair at the 5′ end and an AU base pair at the 3′ end could be shielded by over 2 p.p.m. in an A-RNA helix (32). It is noteworthy, that the signal intensity and the half-width of the G24 imino proton is comparable to other imino signals. No imino proton resonances could be detected for hypothetical A18·U23 and U19·A22 base pairs at temperatures as low as 0°C.

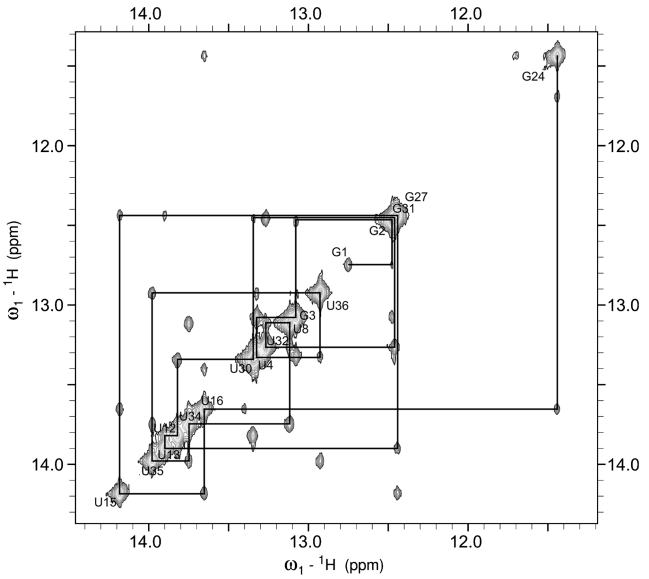

Figure 5. The imino–imino region of the 2D NOESY spectrum (τ_m = 250 ms, 15°C). Lines represent the sequential walk for the base paired region (G1-C17 and G24-C40).

Assignment of resonances

Assignment of imino protons, which established secondary structure was followed by more detailed assignment of non-exchangeable protons (33,34). Pyrimidine H5 protons were identified with the use of 2D DQF-COSY spectra showing through bond correlations with aromatic H6 protons of the same residue. Cytosine H5 protons exhibited strong intranucleotide NOESY correlations with amino protons, which in turn showed NOE cross-peaks to base paired guanine imino protons. Adenine H2 resonances were assigned through their strong NOE correlations with base paired uracil imino protons. Sequential aromatic (H6/H8)-sugar H1′ connectivities could be traced through the whole length of both sense and antisense strands (Figure 6), which enabled us to assign all aromatic and anomeric protons. However, this was done with the help of HF couplings which could be observed in the 2D NOESY spectra. Specifically, scalar couplings of F with H1′ helped us to identify sugar protons belonging to nucleotides with the 2′-F modification. H2′ protons of all 2′-F substituted nucleotides and cca 50% of the H3′ resonances of 2′-F substituted nucleotides could be assigned due to their coupling with fluorine nuclei. Only a few H2′ protons of 2′-OMe substituted nucleotides could be assigned. 2′-OMe proton resonances (in the region from δ3.3 to 3.9 p.p.m.) were assigned by their intra- and internucleotide correlations with aromatic protons. 2D DQF-COSY spectrum showed no H1′-H2′ cross-peaks indicating that the sugar conformations of all nucleotides adopted predominantly N-type puckering. The ^{1}H chemical shift values have been deposited in the Biological Magnetic Resonance data Bank (BMRB, accession no. 16852).

Restraints and structure calculations

NOE distance restraints for non-exchangeable protons were obtained from 2D NOESY spectra recorded at 25°C in 100% ^2H_2O with mixing times ranging from 80 to 250 ms. The volume of the pyrimidine H5-H6 cross-peak was used as the distance reference (2.45 Å). NOE distance restraints for exchangeable protons were obtained from 2D DPFGSE NOESY spectra recorded at 25°C in 5% ^2H_2O, 95% H_2O with mixing time of 250 ms. Cross-peaks were classified as strong (1.8–3.6 Å), medium (2.6–5.0 Å) and weak (3.5–6.5 Å).

Torsion angle restraints for α and ζ were set to 0 ± 120° to exclude *trans* conformations inferred from the narrow range of ^{31}P resonances. Torsion angles ε were restrained to 235 ± 65° to exclude the unfavorable *gauche*$^+$ conformation. Torsion angles β were restrained to 180 ± 40° (*trans*) due to the lack of P-H5′ and P-H5″ cross-peaks in HP-COSY spectrum. The backbone torsion angle restraints (α, β, ε and ζ) were used only for the base paired region (G1-C17, G24-C40). Due to the absence of H1′-H2′ cross-peaks in 2D DQF-COSY spectra, which indicate an N-type sugar pucker, torsion angles δ of all nucleotides were restrained to 85 ± 30°. All torsion angles χ were

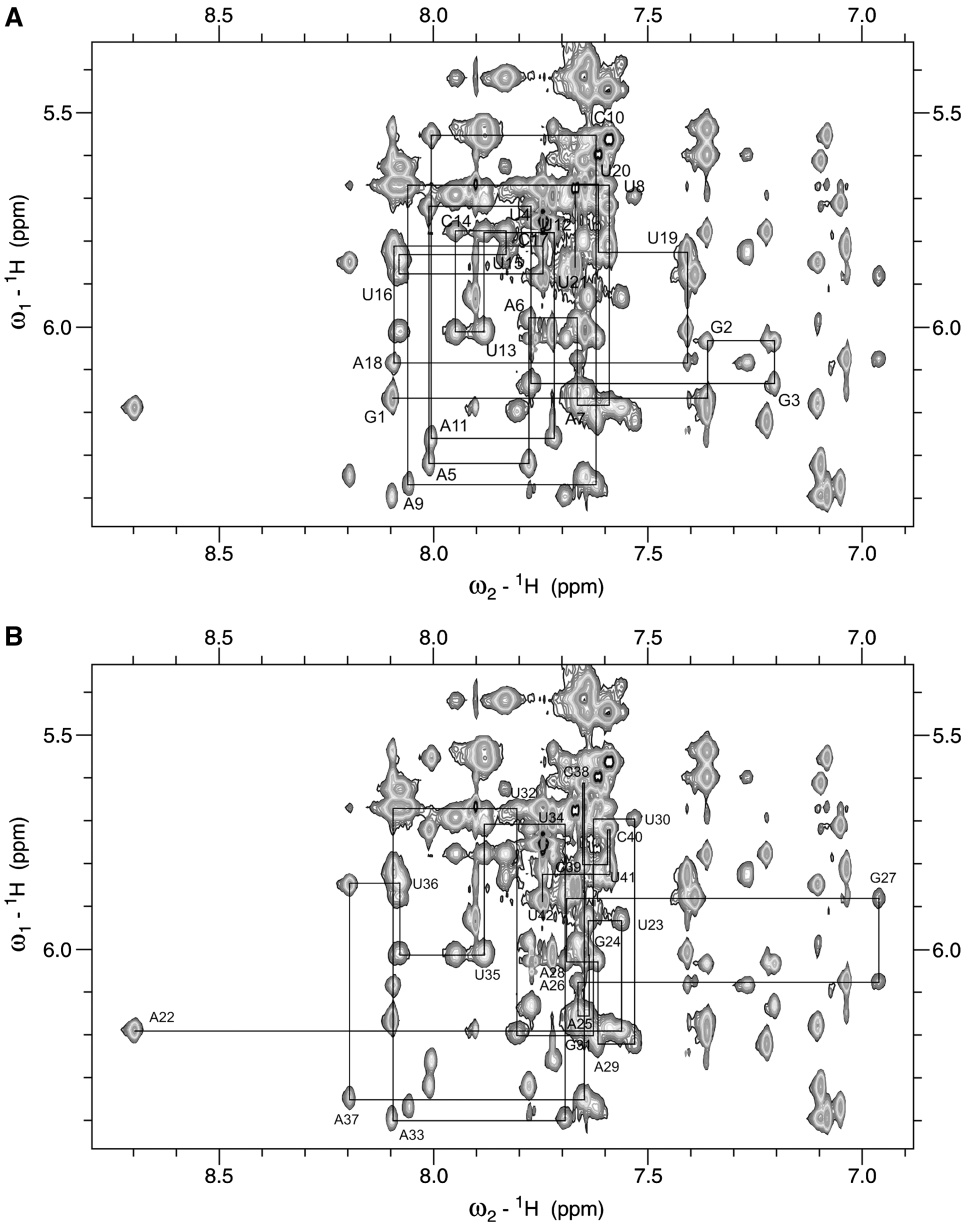

Figure 6. The aromatic–anomeric region of the 2D NOESY spectrum (τ_m = 150 ms, 25°C). Lines represent the sequential walk for the sense, G1-U21 (**A**) and antisense, A22-U42 (**B**) strands, which are shown separately to reduce overlap.

restrained to −120 ± 90° (anti) based on the intensity of intraresidual H6/H8-H1′ NOESY cross-peaks.

The above NOE distance and torsion angle restraints were complemented by the implementation of HF residual dipolar coupling constants (35). The fluorine nucleus (placed on every other nucleotide) is coupled to H1′, H2′ and H3′ sugar protons. Coupling constants were obtained by measuring the HF splittings, which are observable in traces of H1′-H2′ and H2′-aromatic cross-peaks in NOESY spectra. Two bond F-H2′ splittings are in the range from 42.8 to 53.8 Hz and three bond F-H1′ splittings are between 12.1 and 18.8 Hz. After the addition of the Pf1 phages, the splittings were measured again and the RDC values were calculated. We were able to collect F-H1′ and F-H2′ RDC values for all 21 nt, which are 2′-F modified. Measured RDC vales range from 0.7 to 5.2 Hz for F-H2′ and from −0.1 to −3.0 Hz for F-H1′ coupled pair. F-H3′ splittings were observed in NOESY spectra and are in the range from 25 to 30 Hz. However, F-H3′ RDCs could not be determined with sufficient accuracy due to the unreliable measurement of the F-H3′ splitting and severe spectral overlap which limited assignment of H3′ protons.

Finally, 311 NOE restraints, 219 torsion angles and 42 RDCs were used in the structure calculation process (Table 1). Forty hydrogen bond and 34 bp planarity restraints were used for the 17 AU and GC base pairs. No hydrogen bond and planarity restraints were used for the hypothetical A18·U23 and U19·A22 base pairs, for which no imino signals could be observed.

A set of 100 structures was calculated using SA protocol and energy minimization, from which the 10 lowest energy structures were selected. The final set of 10 structures

Table 1. Structural statistics

NOE-derived distance restraints	
Intranucleotide NOEs	135
Sequential NOEs	151
Long-range NOEs	25
Torsion angle restraints	219
Hydrogen bond restraints	40
Base pair planarity restraints	34
Residual dipolar couplings	42
NOE violations >0.3 Å	0
Deviations from idealized covalent geometry	
Bonds (Å)	0.010 ± 0.000
Angles (°)	2.48 ± 0.02
Pairwise heavy atom RMSD (Å)	
Overall	2.29
Without UU overhangs (1–19, 22–40)	1.78
Only the base paired region (1–17, 24–40)	1.54

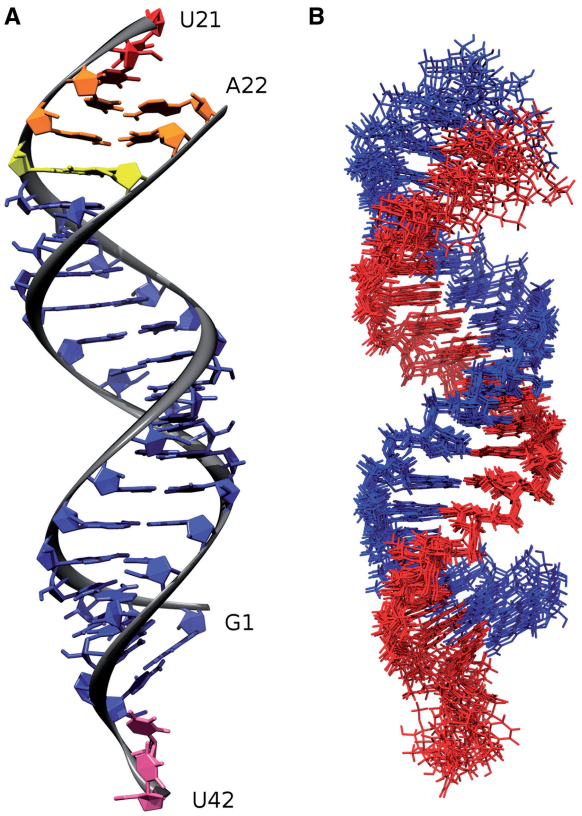

Figure 7. (**A**) The lowest energy structure of the 2′-F/2′-OMe modified dimeric 42-nt RNA construct. Nucleotides G1-U16 and A25-C40 are depicted in blue, base pair C17 G24 is in yellow and base pairs A18 U23 and U19 A22 are in orange. (**B**) Superposition of the 10 lowest energy structures of the 42-nt construct. Sense and antisense strands are in blue and red, respectively.

exhibits a pairwise heavy atom RMSD of 2.3 Å, while the base paired region (G1-C17, G24-C40) alone displays a RMSD of 1.5 Å. The construct adopts an A-type double helical structure (Figure 7) with an average rise and twist parameters of 2.9 Å and 30.5°, respectively. For comparison, the rise and twist parameters in standard A-type RNA are 2.8 Å and 32.8°, respectively (36).

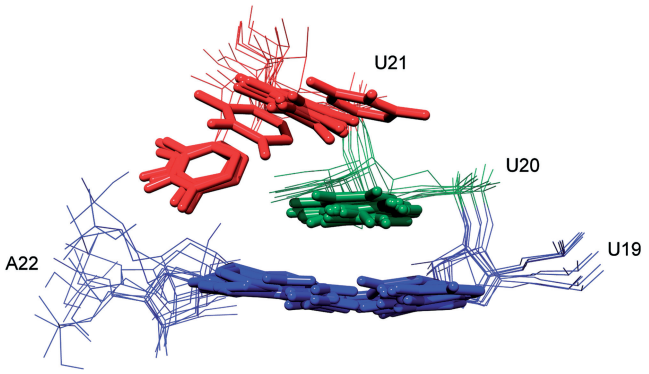

Figure 8. Superposition of the 10 lowest energy structures of the U20, U21 overhang over the U19 A22 base pair.

Perusal of the structures shown in Figure 7 shows the formation of 19 Watson–Crick base pairs in the stem region (G1-U19 and A22-C40). Interestingly, imino proton signals of A18-U23 and U19-A22 base pairs have not been observed experimentally. In accordance, the structure of these two terminal base pairs is less well defined, due to the lack of a hydrogen bond, base planarity and backbone torsion angle restraints. All 2′-OMe groups in the stem region are rotated towards the minor groove. The structure of the U20 and U21 overhang in the sense strand is not well defined. However, in all 10 final structures U20 stacks on the terminal A19·U22 base pair and in several structures U21 stacks on U20 (Figure 8). On the other hand, the U41 and U42 overhang in the antisense strand does not stack on the terminal G1·C40 base pair, instead, 2′-OMe group of C40 is positioned above its pyrimidine ring and blocks stacking of U41. As a result, the U41 and U42 overhang is poorly defined and does not adopt a well defined structure.

DISCUSSION

Short synthetic oligonucleotides can be used to specifically modulate gene expression through the RNA interference (RNAi) mechanism. However, the use of such molecules *in vivo* did not bring expected results, partly due to the low nuclease stability of siRNA oligonucleotides originating from natural nucleotides. Several chemical modifications on the ribose ring were shown to improve pharmacokinetic properties of synthetic oligonucleotides without causing toxicity, which is crucial for delivery of such molecules into living organisms. A completely 2′-F/2′-OMe modified dimeric RNA construct was previously shown to be a highly potent RNAi trigger in HeLa cells (18). In the current study, we present a 3D structure of a 42-nt dimeric alternately 2′-F/2′-OMe modified construct consisting of a Watson–Crick base paired duplex with additional 3′ UU overhangs and a 5′ phosphate group on the antisense strand, which mimics naturally occurring siRNAs produced in cells by the Dicer enzyme.

The two 21-nt oligos efficiently hybridize thus forming an A-type double helix with 3′ UU overhangs on both strands. The helical segment is completely complementary

and exhibits 19 Watson–Crick base pairs. The overall thermal stability of the duplex, reflected by a T_m of 81.7°C, is not appreciably different from the stability of an identical duplex lacking the 3′ UU overhangs, with a previously reported T_m of 82.0°C (18). However, NMR data suggests that the stability of individual base pairs is not uniform throughout the entire length of the construct. Most of the double helix (G1-U16, A25-C40), apart from the last three base pairs, exhibits well dispersed imino resonances in the Watson–Crick region of NMR spectra. However, the last 3 bp display somewhat different properties. G24 imino proton exhibits a chemical shift of δ11.5 p.p.m., which is uncharacteristic for imino protons involved in GC Watson–Crick base pairs. Interestingly, the line-width of this signal is comparable to other imino resonances in the Watson–Crick region. U19 and U23 imino resonances involved in AU base pairs could not be observed in NMR spectra even after lowering the temperature to 0°C, which clearly indicates that these imino protons are accessible to solvent exchange. Differences in stability of helix segments can be attributed to the base pair composition of the construct, which ends with two AU base pairs on one end and with three GC base pairs on the opposite end. Our findings are in agreement with previous reports, which suggest that a difference in stability of duplex ends is required for the incorporation of the correct siRNA strand into RISC (37,38).

During the RISC assembly process, the RISC-loading complex loads the siRNA duplex into Ago2 (39). The 5′ end of the guide strand is inserted into the phosphate binding pocket of the Ago2 PIWI domain and serves as a template for target mRNA recognition. The passenger strand is subsequently cleaved by Ago2 and ejected from the RISC complex. Guide and passenger strands are determined on the basis of relative stabilities of helix ends (37,38). The helix end that is less stable interacts with the PIWI domain of Ago2, which results in the unwinding of the first base pair (40,41). The strand whose 5′ end is at the less stable end of the helix becomes the guide strand, while the other strand becomes the passenger strand. Our data show a clear difference in the relative stability of helix ends. The labile base pairs A18·U23 and U19·A22 suggest that the A22–U42 strand will serve as a guide strand and will thus control the incorporation of the siRNA duplex into the RISC complex.

Although one end of the helix is less stable, the existence of fraying ends in solution can be dismissed due to the presence of several inter-strand NOE cross-peaks correlating aromatic and sugar protons between U20 and A22 (Supplementary Figure S2). All structures obtained by SA simulations exhibit A18·U23 and U19·A22 base pairs, despite the absence of hydrogen bond restraints for these base pairs. Stabilization of these base pairs is probably achieved through favorable stacking interactions. Furthermore, the U20 and U21 overhang in the sense strand stacks efficiently on the terminal U19·A22 base pair.

On the other hand, there is poor, if any, base–base stacking of the U41 and U42 overhang on the terminal GC base pair in the antisense strand. The stacking of U41 is prevented by the 2′-OMe group of C40, which is positioned directly above the aromatic ring of C40. As a result, the structure of the U41, U42 overhang is poorly defined. This appears to have no effect on the terminal GC base pair. Apart from the G1 imino proton signal being slightly broader at 25°C, which is expected due to its exposure to exchange processes at the helix end, there is no indication of exchange of hydrogen bonded imino protons with solvent in the rest of the helix (G1-U16, A25-C40).

For comparison, preliminary measurements on the native isosequential siRNA were performed. The native analogue displays similar features to the 2′-F/2′-OMe modified siRNA. Very good dispersion of the imino proton chemical shifts has been observed (Supplementary Figures S3 and S4). As expected, the G24 imino proton exhibits an upfield chemical shift due to its position between UA and AU base pairs. However, a large part of the aromatic and anomeric proton resonances is condensed in highly overlapped regions, which precludes further analysis with an isotopically unlabeled RNA sample of this molecular weight (Supplementary Figure S5). It is noteworthy that DQF-COSY spectrum showed no cross-peaks in H1′-H2′ region, which is indicative of N-type sugar conformation.

All nucleotides in the construct exhibit a predominantly N-type sugar pucker, which is usually found in RNA molecules. This is partly due to the presence of 2′ modifications, which favor the C3′-endo conformation of the sugar ring (20–22). The RNA like conformation greatly improves the binding affinity for the target RNA, which is desired for synthetic siRNA oligonucleotides. It is not surprising that the introduction of 2′-fluoro and 2′-OMe modifications does not have any significant impact on the structure of the construct. Deviations from the native A-type RNA structure could reduce the efficiency of the RNAi mechanism. The alternating 2′-F/2′-OMe motif appears to be a promising design for synthetic siRNA oligonucleotides with high serum stability.

CONCLUSION

A high-resolution structure of the stable 42-nt RNA dimeric construct has been derived based on a high number of NMR observables including NOEs, J-coupling constants and RDCs. It is amazing that sufficient resolution of NMR signals was achieved on an 800 MHz NMR spectrometer which enabled sequential assignment of a 14 kDa dimer without isotope labeling. The two 21-nt oligos efficiently hybridized thus forming an A-type double helix with 3′ UU overhangs on both strands. Ribose units in siRNA construct were alternately substituted by a 2′-deoxy-2′-fluoro or 2′-methoxy groups which contributed to the stabilization of the N-type sugar conformation that is typically associated with structure of A-form of RNA. Structure calculations utilized a set of H-F RDC values under conditions of weak alignment achieved by Pf1 phages for all 21 nt, which were 2′-F modified. A completely 2′-F/2′-OMe modified dimeric RNA construct adopts an antiparallel double-helical

structure consisting of 19 Watson–Crick base pairs with additional 3′ UU overhangs and a 5′ phosphate group on the antisense strand. NMR data suggests that the stability of individual base pairs is not uniform throughout the construct. While most of the double helical segment exhibits well dispersed imino resonances, the last three base pairs display either uncharacteristic chemical shifts of imino protons involved in a GC Watson–Crick base pair or could not be observed even at lower temperatures. Accessibility of imino protons to solvent exchange suggests a difference in stability of the duplex ends which might be of importance for incorporation of the guide siRNA strand into the RISC.

SUPPLEMENTARY DATA

Supplementary Data are available at NAR Online.

FUNDING

Slovenian research agency (ARRS), Ministry of higher education, science and technology of Republic of Slovenia (program no. P1-0242); EN-FIST Center of Excellence. Funding for open access charge: Slovenian Research Agency (ARRS).

Conflict of interest statement. None declared.

REFERENCES

1. Napoli,C., Lemieux,C. and Jorgensen,R. (1990) Introduction of a chimeric chalcone synthase gene into petunia results in reversible co-suppression of homologous genes in trans. *Plant Cell*, **2**, 279–289.
2. Fire,A., Xu,S., Montgomery,M.K., Kostas,S.A., Driver,S.E. and Mello,C.C. (1998) Potent and specific genetic interference by double-stranded RNA in Caenorhabditis elegans. *Nature*, **391**, 806–811.
3. Elbashir,S.M., Harborth,J., Lendeckel,W., Yalcin,A., Weber,K. and Tuschl,T. (2001) Duplexes of 21-nucleotide RNAs mediate RNA interference in cultured mammalian cells. *Nature*, **411**, 494–498.
4. Elbashir,S.M., Lendeckel,W. and Tuschl,T. (2001) RNA interference is mediated by 21- and 22-nucleotide RNAs. *Gene. Dev.*, **15**, 188–200.
5. Davis,M.E., Zuckerman,J.E., Choi,C.H.J., Seligson,D., Tolcher,A., Alabi,C.A., Yen,Y., Heidel,J.D. and Ribas,A. (2010) Evidence of RNAi in humans from systemically administered siRNA via targeted nanoparticles. *Nature*, **464**, 1067–1070.
6. Zamore,P.D. and Haley,B. (2005) Ribo-gnome: The Big World of Small RNAs. *Science*, **309**, 1519–1524.
7. Rana,T.M. (2007) Illuminating the silence: understanding the structure and function of small RNAs. *Nat. Rev. Mol. Cell. Biol.*, **8**, 23–36.
8. Jinek,M. and Doudna,J.A. (2009) A three-dimensional view of the molecular machinery of RNA interference. *Nature*, **457**, 405–412.
9. Peters,L. and Meister,G. (2007) Argonaute proteins: mediators of RNA silencing. *Mol. Cell*, **26**, 611–623.
10. Bumcrot,D., Manoharan,M., Koteliansky,V. and Sah,D.W.Y. (2006) RNAi therapeutics: a potential new class of pharmaceutical drugs. *Nat. Chem. Biol.*, **2**, 711–719.
11. Behlke,M.A. (2008) Chemical modification of siRNAs for in vivo use. *Oligonucleotides*, **18**, 305–319.
12. Watts,J.K., Deleavey,G.F. and Damha,M.J. (2008) Chemically modified siRNA: tools and applications. *Drug. Discov. Today*, **13**, 842–855.
13. Chiu,Y. and Rana,T.M. (2003) siRNA function in RNAi: a chemical modification analysis. *RNA*, **9**, 1034–1048.
14. Cummins,L.L., Owens,S.R., Risen,L.M., Lesnik,E.A., Freier,S.M., McGee,D., Guinosso,C.J. and Cook,P.D. (1995) Characterization of fully 2′-modified oligoribonucleotide hetero- and homoduplex hybridization and nuclease sensitivity. *Nucleic Acids Res.*, **23**, 2019–2024.
15. Kawasaki,A.M., Casper,M.D., Freier,S.M., Lesnik,E.A., Zounes,M.C., Cummins,L.L., Gonzalez,C. and Cook,P.D. (1993) Uniformly modified 2′-deoxy-2′-fluoro-phosphorothioate oligonucleotides as nuclease-resistant antisense compounds with high affinity and specificity for RNA targets. *J. Med. Chem.*, **36**, 831–841.
16. Prakash,T.P. and Bhat,B. (2007) 2-modified oligonucleotides for antisense therapeutics. *Curr. Top. Med. Chem.*, **7**, 641–649.
17. Vickers,T.A., Koo,S., Bennett,C.F., Crooke,S.T., Dean,N.M. and Baker,B.F. (2003) Efficient reduction of target RNAs by small interfering RNA and RNase H-dependent antisense agents. *J. Biol. Chem.*, **278**, 7108–7118.
18. Allerson,C.R., Sioufi,N., Jarres,R., Prakash,T.P., Naik,N., Berdeja,A., Wanders,L., Griffey,R.H., Swayze,E.E. and Bhat,B. (2005) Fully 2′-modified oligonucleotide duplexes with improved in vitro potency and stability compared to unmodified small interfering RNA. *J. Med. Chem.*, **48**, 901–904.
19. Davis,S., Propp,S., Freier,S.M., Jones,L.E., Serra,M.J., Kinberger,G., Bhat,B., Swayze,E.E., Bennett,C.F. and Esau,C. (2009) Potent inhibition of microRNA in vivo without degradation. *Nucleic Acids Res.*, **37**, 70–77.
20. Plavec,J., Tong,W. and Chattopadhyaya,J. (1993) How do the gauche and anomeric effects drive the pseudorotational equilibrium of the pentofuranose moiety of nucleosides? *J. Am. Chem. Soc.*, **115**, 9734–9746.
21. Thibaudeau,C., Plavec,J. and Chattopadhyaya,J. (1994) Quantitation of the anomeric effect in adenosine and guanosine by comparison of the thermodynamics of the pseudorotational equilibrium of the pentofuranose moiety in N- and C-nucleosides. *J. Am. Chem. Soc.*, **116**, 8033–8037.
22. Thibaudeau,C. and Chattopadhyaya,J. (1999) *Stereoelectronic Effects in Nucleosides and Nucleotides and their Structural Implications*. Uppsala University Press, Uppsala, Sweden.
23. Polak,M., Manoharan,M., Inamati,G.B. and Plavec,J. (2003) Tuning of conformational preorganization in model 2′,5′- and 3′,5′-linked oligonucleotides by 3′- and 2′-O-methoxyethyl modification. *Nucleic Acids Res.*, **31**, 2066–2076.
24. Plevnik,M., Gdaniec,Z. and Plavec,J. (2005) Solution structure of a modified 2′,5′-linked RNA hairpin involved in an equilibrium with duplex. *Nucleic Acids Res.*, **33**, 17491–759.
25. Wang,Y., Sheng,G., Juranek,S., Tuschl,T. and Patel,D.J. (2008) Structure of the guide-strand-containing argonaute silencing complex. *Nature*, **456**, 209–213.
26. Wang,Y., Juranek,S., Li,H., Sheng,G., Tuschl,T. and Patel,D.J. (2008) Structure of an argonaute silencing complex with a seed-containing guide DNA and target RNA duplex. *Nature*, **456**, 921–926.
27. Perez,A., Marchan,I., Svozil,D., Sponer,J., Cheatham,T., Laughton,C. and Orozco,M. (2007) Refinement of the AMBER force field for nucleic acids: improving the description of α/γ conformers. *Biophys. J.*, **92**, 3817–3829.
28. Venkateswarlu,D. and Ferguson,D.M. (1999) Effects of C2'-substitution on arabinonucleic acid structure and conformation. *J. Am. Chem. Soc.*, **121**, 5609–5610.
29. Aduri,R., Psciuk,B.T., Saro,P., Taniga,H., Schlegel,H.B. and SantaLucia,J. (2007) AMBER force field parameters for the naturally occurring modified nucleosides in RNA. *J. Chem. Theory Comput.*, **3**, 1464–1475.
30. Lu,X. and Olson,W.K. (2003) 3DNA: a software package for the analysis, rebuilding and visualization of three-dimensional nucleic acid structures. *Nucleic Acids Res.*, **31**, 5108–5121.
31. Zuker,M. (2003) Mfold web server for nucleic acid folding and hybridization prediction. *Nucleic Acids Res.*, **31**, 3406–3415.
32. Patel,D.J. and Tonelli,A.E. (1975) Nuclear magnetic resonance investigations of the structure of the self-complementary duplex of d-ApTpGpCpApT in aqueous solution. *Biochemistry*, **14**, 3990–3996.

33. Wijmenga,S.S. and van Buuren,B.N.M. (1998) The use of NMR methods for conformational studies of nucleic acids. *Prog. Nucl. Mag. Res. Sp.*, **32**, 287–387.
34. Fürtig,B., Richter,C., Wöhnert,J. and Schwalbe,H. (2003) NMR spectroscopy of RNA. *ChemBioChem.*, **4**, 936–962.
35. Luy,B. and Marino,J. (2001) Measurement and application of 1H-19F dipolar couplings in the structure determination of 2′-fluorolabeled RNA. *J. Biomol. NMR*, **20**, 39–47.
36. Saenger,W. (1984) *Principles of Nucleic Acid Structure*. Springer, New York, NY.
37. Schwarz,D.S., Hutvágner,G., Du,T., Xu,Z., Aronin,N. and Zamore,P.D. (2003) Asymmetry in the assembly of the RNAi enzyme complex. *Cell*, **115**, 199–208.
38. Khvorova,A., Reynolds,A. and Jayasena,S.D. (2003) Functional siRNAs and miRNAs exhibit strand bias. *Cell*, **115**, 209–216.
39. Matranga,C., Tomari,Y., Shin,C., Bartel,D.P. and Zamore,P.D. (2005) Passenger-strand cleavage facilitates assembly of siRNA into Ago2-containing RNAi enzyme complexes. *Cell*, **123**, 607–620.
40. Parker,J.S., Roe,S.M. and Barford,D. (2005) Structural insights into mRNA recognition from a PIWI domain-siRNA guide complex. *Nature*, **434**, 663–666.
41. Ma,J., Yuan,Y., Meister,G., Pei,Y., Tuschl,T. and Patel,D.J. (2005) Structural basis for 5′-end-specific recognition of guide RNA by the A. fulgidus Piwi protein. *Nature*, **434**, 666–670.